Characterizing fire effects on conifers at tree level from airborne laser scanning and high-resolution, multispectral satellite data

Carine Klauberg[a,b,*], Andrew T. Hudak[b], Carlos Alberto Silva[c,d], Sarah A. Lewis[b], Peter R. Robichaud[b], Terrie B. Jain[b]

[a] Federal University of São João Del Rei – UFSJ, Sete Lagoas, MG 35701-970, Brazil
[b] USDA Forest Service, Rocky Mountain Research Station, 1221 South Main Street, Moscow, ID 83843, USA
[c] Biosciences Laboratory, NASA Goddard Space Flight Center, Greenbelt, MD 20707, USA
[d] Department of Geographical Sciences, University of Maryland, College Park, MD 20740, USA

ABSTRACT

Post-fire assessment is made after a wildfire incident to provide details about damage level and its distribution over burned areas. Such assessments inform restoration plans and future monitoring of ecosystem recovery. Due to the high cost and time to conduct fieldwork, remote sensing is an appealing alternative to assess post-fire condition over larger areas than can be surveyed practically in the field. The aim of this study is to use remote sensing data to characterize post-fire severity at tree level in a mixed conifer forest following the Cascade and East Zone megafires of 2007 in central Idaho, USA. We used remote sensing metrics derived from Airborne Laser Scanning (ALS) data (2008) and high-resolution QuickBird (QB) multispectral satellite imagery (2007–2009) for calibrating and validating predictive models with field data (2008). We compared fire effects on trees in open canopies within recent fuel treatments to similar trees in closed canopies on adjacent, untreated sites. We observed more trees with charred crowns in high fire severity sites, mostly untreated, whereas we observed more trees with live crowns in low fire severity sites, independent of the treatment. Individual trees were more accurately detected from ALS data in treated sites with open canopies than untreated sites with closed canopies. For detected trees, the response variables predicted from ALS and QB metrics were total height (Ht), crown base height (CBH), total basal area (BA_T), live basal area (BA_L), scorched basal area (BA_S), charred basal area (BA_C) and crown severity (CS). None of the selected QB metrics were strongly correlated with the selected ALS metrics, which justified combining both data types into the predictive models. Random Forest regression models combining ALS + QB metrics or using ALS metrics alone performed similarly but clearly better than models using only QB metrics. This study shows the superiority of ALS data to high resolution, multispectral QB imagery for mapping fire severity at tree level. Managers with limited resources to plan for restoration of fire affected forests are advised to prioritize spending for data collection on ALS data and a modest number of field inventory plots, rather than QB or other broadband satellite imagery.

1. Introduction

Wildfires suppression in the western U.S. costs billions of dollars annually and places firefighters and the public at risk (NIFC, 2019). Many advocate an increase in fuel treatment implementation to alter fire behavior and effects and promote successful fire suppression at a lower cost (e.g., Cohen, 2000; Lentile et al., 2006; Ellison et al., 2015; Hudak et al., 2011a; Swetnam et al., 2015). Over the last 20 years, efforts to alter hazardous fuels have been ongoing with emphasis on treating areas where people and their property reside, often referred to as the Wildland Urban Interface (WUI). It is assumed that these fuel treatments will alter fire behavior and severity to allow for fire suppression opportunities and produce post-fire outcomes that are socially acceptable. Fuel treatments are designed to reduce hazardous fuels focus on four forest structural and compositional characteristics that include altering surface fuels, ladder fuels, crown fuels, and shifting species composition (Agee and Carl, 2005), but in some cases are not sociable acceptable in all conditions (Molina-Terrén et al., 2016). Surface fuels typically are treated either through prescribed fire, grapple piling, or mastication. Thinning tree crowns and thinning from below are applied to separate crowns and remove ladder fuels. Fire-resistant species are often favored over non-fire-resistant species (Graham et al.,

2004; Hurteau and North, 2010). These treatments are designed to reduce fire behavior and mitigate fire severity in case a wildfire occurs. However, there are mixed results indicating as to whether fuel treatments alter fire effects when a wildfire does burn through these treatments (Hudak et al., 2011a). Another reason is that research on fuel treatment effectiveness is still needed because the frequency that a wildfire will test a fuel treatment is low as a percentage of the fuel treatments implemented.

Most large wildfires have a post-fire assessment to inform managers on where and how much the fire affected the soils and vegetation. Fire severity can be either defined to the loss or decomposition of organic matter aboveground and belowground (Keeley, 2009) as the first-order fire effects, such as how much of the duff, logs, and other dense organic matter on the soil surface is consumed (Ice et al., 2004). For trees, as suggested by Hudak et al. (2007), sites may be classified as low severity when live (green) crowns are predominate, as moderate severity when scorched (brown) crowns are predominant, and as high severity when charred (black) crowns predominate. The spatial distribution of fire severity and consequently the identification of the tree crown severity class (live, scorched or charred) are key factors that may be used to quantify the impact of fires and vegetation response, and consequently guide post-fire management responses(Montealegre et al., 2014). Knowledge about the crown severity of each tree helps to predict future site conditions. Given that mapped tree crowns capture the spatial distribution of trees, tree crown severity maps could be used to develop more precise, site-specific forest and fire management plans (Kim et al., 2009). Remote sensing tools have potential to assess post-fire impacts on vegetation structure and physiology, which is important to understand the fire severity effects on post-fire ecosystem processes in small areas (i.e., plots and pixels) or at the tree level using high resolution data (Kokaly et al., 2007).

The use of remote sensing data to understand fire effects over large areas has been well studied at the landscape level using moderate resolution (e.g., Landsat) satellite imagery (e.g., Miller and Yool, 2002; Miller and Thode, 2007; Hudak et al., 2007; French et al., 2008; Verbyla and Lord, 2008; Veraverbeke et al., 2011). Prior studies typically involved identification of unique spectral signatures associated with burn areas (Holden et al., 2010) or snags (Pasher and King, 2009), or the use of combined spectral and texture features to identify forest gaps (Barton et al., 2017). Although satellite remote sensing has been shown to be an essential technology for studying post-fire consequences, the traditional and older generation sensors such as Landsat and SPOT have a number of limitations with regard to spectral, spatial and temporal resolution (Steininger, 2000). These limitations might be overcome using a newer generation of sensors with higher spatial resolution such as QuickBird (QB) to more accurately resolve smaller landscape features, including trees. Spectral vegetation indices such as Normalized Difference Vegetation Index (NDVI, Tucker, 1979) and Red-Green Index (RGI, Coops et al., 2006) can be used to differentiate live trees from dead trees. High resolution imagery also has been used to detect burn severity from wildfire (Holden et al., 2010; Holden et al., 2012). Recognition of fire-affected tree attributes such as percent of live, scorched, or charred crown may facilitate the selection of which trees to salvage, or to leave as potential seed sources (Lentile et al., 2006). In addition, wildlife habitat relationships can be mapped, validated, and improved when habitat components such as live, scorched, and charred crown trees are spatially mapped, which is a valuable step for management and conservation applications (Vogeler et al., 2016).

The combined use of high-resolution, passive optical multispectral imagery with active sensors could provide more accurate post-fire information than either sensor type alone. Fire severity estimations from active sensors are more sensitive to disturbance effects on forest structure than passive satellite sensors (McCarley et al., 2017). Examples of active sensors include Radio Detection and Ranging (radar) and Light Detection and Ranging (lidar) (Tanase et al., 2010, 2011; Kane et al., 2013). Airborne lidar (also known as Airborne Laser

Scanning - ALS) is an example of an active remote sensing technology capable of simultaneously characterizing terrain and vegetation structure across large spatial extents (Hudak et al., 2009). ALS has increased the accuracy and efficiency of large-scale forest inventories and wildlife habitat studies (Næsset, 2002; Maltamo et al., 2006; Martinuzzi et al., 2009).. ALS data have been used in fire studies to estimate fuel parameters to use as input into fire behavior models, such as crown bulk density or height to live crown (Andersen et al., 2005; Agca et al., 2011; Skowronski et al., 2011), as well as to assess changes in forest structure (Wulder et al., 2009; McCarley et al., 2017). Although ALS data are limited in spatial and temporal coverage and come at a relatively high cost to project managers (Vogeler et al., 2016), their rich 3-D information of forest structure make them relevant for a variety of natural resource management applications (Hudak et al., 2009).

Numerous studies have explored combining multiple remote sensing datasets and corresponding field data for modeling forest attributes (e.g., Hudak et al., 2006; Dalponte, 2018; Goetz et al., 2010; Bright et al., 2012; Bright et al., 2014). However, few studies have tested this combination in the post-fire environment and at the individual tree level (Wulder et al., 2009; Swetnam et al., 2015; Casas et al., 2016) between treated and untreated stands. The objective of this study was to characterize post-fire total crown height (Ht), crown base height (CBH), total basal area (BA_T), live basal area (BA_L), scorched basal area (BA_S), charred basal area (BA_C) and crown severity (CS) classes at tree level in a mixed conifer forest from one-year post-fire ALS and either immediate, one-year or two-year post-fire high-resolution, multispectral QB images.

2. Methods

2.1. Study area

The study focuses on Secesh Meadows and Warm Lake, two forested communities in the wildland-urban interface (WUI) of central Idaho that had been protected with WUI and Firewise fuel treatments prior to the Cascade and East Zone megafires of 2007 (Graham et al., 2009; Hudak et al., 2011a,b). The WUI treatments were implemented from 2000 to 2006 on National Forest lands on the outskirts of both communities (Fig. 1), whereas Firewise treatments (not shown) were implemented on the private lands. Pile and burn fuel treatments were implemented at Secesh Meadows, while at Warm Lake there was a mix of pile and burn, mastication, and underburn treatments (Hudak et al., 2011a).

2.2. Field data collection

Trees (n = 880) were tallied in August 2008 using 20 paired plots designed to assess effectiveness of mechanical fuel treatments for mitigating severe wildfire effects (Hudak et al., 2011a). The treated plot of each pair was randomly located inside the treatment unit, whereas the untreated plot was situated in a random location with a similar slope and aspect just outside the treatment unit (Fig. 1). Thirteen paired plots (i.e., n = 26) were situated in the Secesh Meadows study area while seven paired plots (i.e., n = 14) were situated in the Warm Lake study area. Each plot was 0.04 ha in area (11.3 m radius). All trees > 12 cm were tallied for diameter at breast height (DBH), species, and live/dead status. From DBH, total basal area was calculated (BA_T). On a subsample of trees, comprised of the largest and smallest tree of each species in each plot quadrant, the Ht and CBH was measured, while percentages of live, scorched, and charred tree crown were visually estimated and recorded with 5% precision under the constraint that they sum to 100% (Hudak et al., 2011a).

2.3. Tree attribute imputation

We applied *k*-Nearest Neighbor (*k*-NN) imputation, a nonparametric
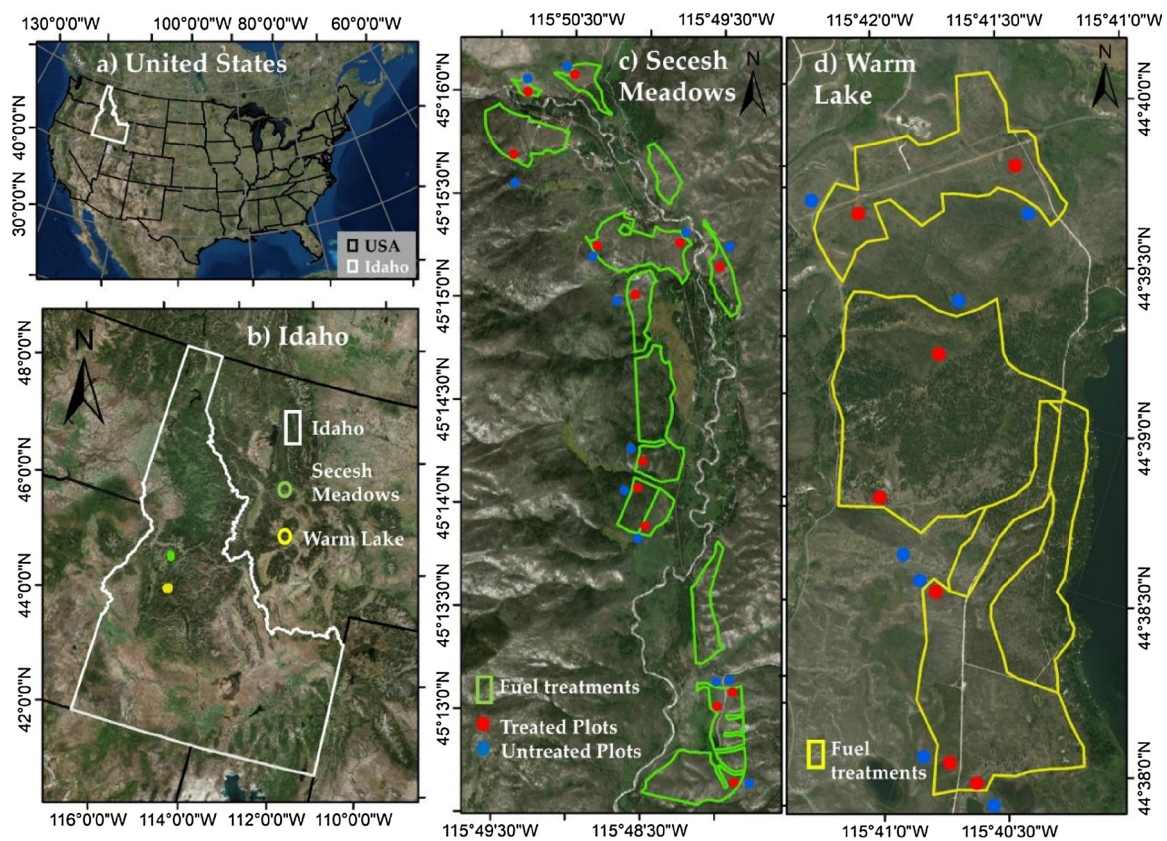
Fig. 1. Map of the study area in central Idaho, USA. Image source: ESRI (2011).

modeling technique, to infer missing values of the subsampled tree attributes [Ht, CBH, and percentages of live, scorched and charred crowns], using the yaImpute package (Crookston and Finley, 2008) in the R statistical software (R Core Team, 2019). For this study, we used Random Forest based k-NN (RF k-NN) imputation to infer the missing tree attributes from predictor variables known for all trees tallied in the field plots: tree DBH, species, study area (Secesh Meadows or Warm Lake), site condition (treated or untreated), and site fire severity as called on the ground for the site (low, moderate or high). The number of neighbors was set to one ($k = 1$) to maintain the original variance in the data (Hudak et al., 2008).

2.4. QuickBird imagery acquisition and pre-processing

QuickBird images were acquired immediately after the wildfire on 22 October (Secesh Meadows) and 27 October (Warm Lake) 2007 and again on 18 August 2008 (Warm Lake) and on 16 July 2009 (Secesh Meadows). The 2007 images capturing immediate fire effects and collected only 5 days apart were considered for the main analysis of this study, whereas the later images also considered are detailed in the supplementary material. The four 2.4 m multispectral bands were fused with the 0.6 m panchromatic band into a 4-band product of 0.6 m resolution delivered by the vendor (DigitalGlobe, Longmont, CO). Several vegetation indices with potential sensitivity to fire effects were calculated from the 0.6 m fused 4-band QB imagery (Table 1).

2.5. Airborne laser scanning acquisition and pre-processing

Airborne Laser Scanning (ALS) data were collected over the two study areas (Secesh Meadows and Warm Lake) one year after the wildfire on 1–3 September 2008 (Table 2). The ALS vendor [Watershed Sciences (now Quantum Spatial), Inc., Portland, OR] post-processed and delivered the data as LAS files. Returns were classified using the

lasground function in LAStools (Isenburg, 2018), and a 1 m resolution digital terrain model (DTM) was interpolated from the ground returns using the gridsurfacecreate function in FUSION software (McGaughey, 2018). The point clouds were height normalized by subtracting the elevation of the DTM at each point, and the canopy height model (CHM) was created from the normalized heights at 0.5 m resolution.

2.6. Individual tree detection

Individual tree detection and crown metrics computation were performed using the rLiDAR package (Silva et al., 2015,2016) in R (R Core Team, 2019) in four steps. First, the 0.5 m CHM was smoothed by a 3 × 3 mean filter to remove spurious local maxima caused by tree branches. Second, individual trees were detected from the smoothed CHM using a local maxima algorithm implemented in the FindTreesCHM function. The FindTreesCHM searched for treetops in the CHM via a moving window with a fixed treetop window size (TWS). A TWS of 5 × 5 was found to be most effective for individual tree detection according to preliminary tests. Third, each individual tree crown was delineated based on Voronoi tessellation (Aurenhammer, 1991) implemented in the ForestCAS function. The crown area (C_{AREA}, m²) was defined from the circle calculated as πr^2, with the radius, r, being half the diameter of the delineated tree crown.

2.7. QB- and ALS-derived crown metrics

The mean and standard deviation of each QB band and spectral index (Table 1, Table S1) at crown level were calculated as candidate variables for the predictive models. For crown metrics derived from ALS data, all returns of the normalized heights within simplified crown polygons were extracted and crown height metrics (e.g., maximum height, mean height, etc., Table 3) were computed using the Crown-Metrics function in rLiDAR (Silva et al., 2015,2016) for each tree

Table 1

Spectral bands and indices from QuickBird imagery. The mean and standard deviation of each band or index were tested as candidate QB metrics at the tree crown level (Table S1).

Spectral Index	Abbreviation	Wavelength/Equation	Reference
Blue	B	450-520 nm	QuickBird imagery
Green	G	520-600 nm	
Red	R	630-690 nm	
Near-Infrared	NIR	760-900 nm	
Normalized Difference Vegetation Index	NDVI	$\frac{NIR - R}{NIR + R}$	(Tucker, 1979)
Enhanced Vegetation Index	EVI	$\frac{2.5(NIR - R)}{(1 + NIR + (6R - 7.5B))}$	(Huete et al., 2002)
Soil Adjusted Vegetation Index	SAVI	$\frac{(NIR - R)}{NIR + R + L} * (1 + L)$ With L = 0.5	(Huete, 1988)
Modified Soil Adjusted Vegetation Index	MSAVI2	$\frac{(2NIR + 1 - \sqrt{(2NIR + 1)^2 - 8(NIR - R)})}{2}$	(Qi et al., 1994)
Burned Area Index	BAI	$\frac{1}{(0.1 + R)^2 + (0.06 + NIR)}$	(Chuvieco 2002)
Red-Green Index	RGI	$\frac{R}{G}$	(Coops et al., 2006)
Blue-Red Index	BRI	$\frac{B}{R}$	(Hart and Veblen, 2015)
Simple Ratio Index	SRI	$\frac{NIR}{R}$	(Davranche et al., 2010)

Table 2

ALS collection parameters.

Parameter	Values
Scanning angle (°)	± 14
Pulse rate (kHz)	≥ 4
Pulse footprint (cm)	< 15
Operating altitude (m)	900
Average point density (points m^{-2})	5

Table 3

ALS-derived tree crown metrics (adapted from Silva et al., 2015).

Abbreviation	Definition
H_{MAX} (m)	Maximum crown height
H_{MEAN} (m)	Mean crown height
H_{SD} (m)	Crown height standard deviation
H_{SKE}	Skewness of Heights
H_{KUR}	Kurtosis of Heights
H_{RANGE}	H_{max}-H_{min}
H_{QR}	Interquartile range (H_{75}-H_{25})
H_{25TH} (m)	Crown height 25th percentile
H_{50TH} (m)	Crown height 50th percentile
H_{75TH} (m)	Crown height 75th percentile
H_{90TH} (m)	Crown height 90th percentile
H_{95TH} (m)	Crown height 95th percentile
H_{99TH} (m)	Crown height 99th percentile
CL (m)	Crown length (H_{MAX} – CBH)
CBH (m)	Crown base height
C_{RATIO}	Crown ratio (CL/ H_{MAX})
C_{AREA} (m^2)	Crown area (π*CRAD^2)
CV (m^3)	Crown volume as the convex hull 3D
CSA (m^2)	Crown surface area as the convex hull 3D
C_{DENS} (%)	Crown Density (returns ≥ CBH / total returns, as a percentage)
I_{MAX}	Maximum intensity
I_{MEAN}	Mean intensity
I_{SD}	Intensity standard deviation
I_{SKE}	Skewness of intensities
I_{KUR}	Kurtosis of intensities
I_{RANGE}	I_{max}-I_{min}
I_{QR}	interquartile range (I_{75}-I_{25})
I_{25TH}	Intensity height 25th percentile
I_{50TH}	Intensity height 50th percentile
I_{75TH}	Intensity height 75th percentile

detected. Based on vertical profiles of the heights within the crown polygon, the normalmixEM function from the mixtools package (Benaglia et al., 2009) in R was fitted to compute crown base height

(CBH, m) from lidar. Crown volume (CV, m^3) and crown surface area (CSA, m^2) were calculated as the volume and surface area of 3D convex hulls derived from all ALS returns within the crown segments (Table 3). Also, intensity metrics were calculated as candidate variables for predictive modeling. As for the effects of the incidence angle on the intensity, several studies have shown that for small angles (up to 15°), this effect can be neglected (Coren and Sterzai, 2006; Kukko et al., 2008). The variables described above were then used to predict the post-fire tree attributes measured in the field [i.e., Ht and CBH] or calculated from the field data [i.e., by multiplying BA_T by the live, scorched, and charred crown percentages to calculate weighted estimates of BA_L, BA_S, BA_C. Also, the live, scorched, and charred percentages were used to classify individual tree crown severity into classes (Table 4).

2.8. Predictive modeling and assessment

Tree stems were not mapped in the field plots, but were sorted beginning north of plot center and proceeding clockwise. Therefore, tree lists tallied in the field or from tree-level ALS metrics were matched based on their total tree height, in a process similar to imputation. First, both the field and ALS individual tree lists for each plot were sorted by total tree height and combined into a single table. Second, if the number of ALS-detected trees was higher than in the field, extra trees were randomly pulled from the ALS-detected tree list within the same plot, or if the number of ALS-detected trees was lower than in the field, trees were randomly added from the ALS-detected tree list within the same plot. Thus, the same number of ALS-derived crown attributes were obtained as trees tallied in the field. This ensured that there were no missing values in the dataset to interfere with the subsequent modeling, and that the tree tally reflected actual tree density on the ground, as this greatly influences fire behavior and severity.

2.8.1. Variable selection and regression modeling

Model Improvement Ratio (MIR) (e.g. Evans and Cushman, 2009; Evans et al., 2010; Evans, 2018; Silva et al., 2017) was applied to identify the most important ALS and QB metrics for predicting Ht, CBH, BA_T, BA_L, BA_S, and BA_C. To create parsimonious models, we reserved only the metrics that exhibited MIRs ≥ 0.35. For modeling, we split the data into training (75%, n = 660) and validation (25%, n = 220) datasets, and the attributes of interest (Ht, CBH, BA_T, BA_L, BA_S, BA_C, and CS classes 1–4) were predicted at the tree level using the training dataset and again the Random Forest package (Breiman, 2001; Liaw and Wiener, 2015) in R. As in the predictor variable selection procedure, ntree was set to 1000 and mtry was set to 2.

Table 4
Tree-level crown severity (CS) classification, adapted from Jain and Graham (2007).

Fire Severity Class	Classification	Description
CS-1 (live)	81% to 100% green	Entire crown comprised of live needles (no sign of fire).
CS-2 (mixed)	45% to 80% green	Crown dominated by live needles but with the presence of scorched needles and/or charred crowns (charred branches with all needles consumed by the fire).
CS-3 (scorched)	56% to 100% brown	Crown dominated by scorched needles but with the presence of some live or charred branches.
CS-4 (charred)	55% to 100% black	Crown dominated by charred branches with only a trace of scorched needles.

For Random Forest regression, the accuracy of estimates for each model was evaluated in terms of Adj.R^2, absolute and relative Root Mean Square Error (RMSE), and Bias based on the linear relationship between predicted and observed values:

$$RMSE \ (m, m^2) = \sqrt{\sum_{i=1}^{n} (\hat{y}_i - y_i)^2/n} \tag{1}$$

$$Bias \ (m, m^2) = \frac{1}{n}\sum_{i=1}^{n} (\hat{y}_i - y_i) \tag{2}$$

Where n is the number of observations, y_i is the observed value for tree properties i, and $\hat{y}_i$ is the predicted value for tree properties i. Moreover, relative RMSE (%) and Bias (%) were calculated by dividing the absolute values (Eqs. 1 and 2) by the mean of the observed values.

The Adj.R^2, absolute and relative RMSE and Bias statistics were computed based on the linear relationship between predicted and observed variables using the validation dataset withheld from training. We used the two-sided Wilcoxon–Mann–Whitney rank-sum (W) (Hollander and Wolfe, 1973; Bauer, 1972) in R to assess if the mean of predicted and the observed crown attributes (i.e., Ht, CBH, BA_T, BA_L, BA_S and BA_C) differed at a significance level of 5%.

2.8.2. Classification modeling and assessment

We ran Random Forest in classification mode to predict the categorical response variable of CS class. To assess the accuracy and precision of the CS classification models, Cohen's Kappa coefficient, and accuracy, sensitivity, and specificity values were calculated. Cohen's Kappa coefficient (Table 5) classifies the model according to the level of agreement and the percentage of data that are reliable.

Classification accuracy shows how often the classifier is correct by equation (TP + TN)/total, where TP is true positive (cases in which "yes" was predicted, and it was true) and TN is true negative (cases in which "no" was predicted and it was true). Sensitivity is defined as the proportion of positive results out of the number of samples which were actually positive. Specificity is defined as the proportion of negative results out of the number of samples which were actually negative.

3. Results

3.1. Evaluation of fuel treatment effectiveness

Field measurements affirmed that the treated sites had fewer trees per hectare (number) than the untreated sites (number). On sites classified as high severity, untreated plots were dominated by charred trees both in total number and percent of trees, while treated plots had

Table 5
Description of Cohen's Kappa coefficient used to assess the (CS) classification.

Value of Kappa	Level of agreement	% of data that are reliable
< 0	None	0–4
0.01–0.20	Minimal	4–15
0.21–0.40	Weak	15–35
0.41–0.60	Moderate	36–63
0.61–0.80	Strong	64–81
0.81–0.99	Almost perfect	82–100

Adapted from: Viera and Garrett (2005).

similar abundance in trees with scorched crowns and charred crowns. Although the moderate severity class in treated stands were dominated by trees with scorched needles, there were a few trees of mixed crown severity, in contrast very few trees had a mixed crown severity in the untreated stands. The low severity class in untreated stands was dominated by live trees versus in treated stands, where there tended to be a diversity of crown damage (Fig. 2).

3.2. Imputation of tree attributes

Individual tree Ht was imputed with comparable precision between treated and untreated sites, although accuracy was higher at treated sites (Table 6). While CBH was imputed with clearly higher precision and accuracy at treated sites than untreated sites (Table 6), percent live and charred crowns were more precisely and accurately imputed at untreated sites than treated sites. But, in general, percent scorched crown was imputed with less precision but more accuracy whether or not the site was treated (Table 6).

3.3. Individual Tree Detection using ALS data

Individual tree detection performed highly better in treated plots with open canopy structure than untreated plots with typically closed canopies. Even though the untreated plots had higher tree density than treated plots, when considering two untreated plots as outliers, the comparison of observed and detected tree density resulted in an increased R^2 of 0.41 (Fig. 3).

3.4. Crown metrics and variable selection

A total of 15 of the 30 candidate ALS metrics (H_{MAX}, H_{MEAN}, H_{SD}, H_{KUR}, H_{QR}, H_{RANGE}, H_{25TH}, I_{MEAN}, I_{SD}, I_{QR}, I_{25TH}, C_{DENS}, CL, CBH, C_{RATIO}), and 6 of the 24 candidate QB metrics ($NDVI_{MEAN}$, $NDVI_{SD}$, EVI_{MEAN}, BAI_{MEAN}, RGI_{MEAN}, RED_{MEAN}) were not highly correlated (i.e., r < 0.9) with at least one other metric within each sensor type group, and therefore were considered further in the MIR analyses. When comparing ALS to QB metrics, the correlations were weak. For instance, $NDVI_{MEAN}$ produced weak and positive correlations with the intensity metrics from ALS, as did I_{25TH}, I_{SD}, I_{MEAN}, and I_{QR} (Fig. 4).

3.5. Random forest modeling and assessment

3.5.1. Regression model

Random Forest models explained 12%–66% of variation in predicting Ht, based on the full dataset (Table 8). However, the models based on the training dataset (75%) performed differently between treated and untreated plots (Figs. 5–7), when assessed with the withheld data (25%). The H_{MAX} and H_{MEAN} metrics were important predictors of Ht in the ALS and ALS + QB models, six indices (BAI_{MEAN}, EVI_{MEAN}, $NDVI_{MEAN}$, $NDVI_{SD}$, RED_{MEAN}, RGI_{MEAN}) were important predictors in the QB model (Table 7). H_{MAX} exhibited the highest MIR in Ht models using ALS metrics or ALS + QB metrics, while the red band exhibited the highest MIR in the Ht model using only QB metrics (Table 7). ALS intensity metrics were not important predictors of Ht in ALS or ALS + QB models. QB metrics were not important as explanatory variables of Ht in ALS + QB models (Table 8).
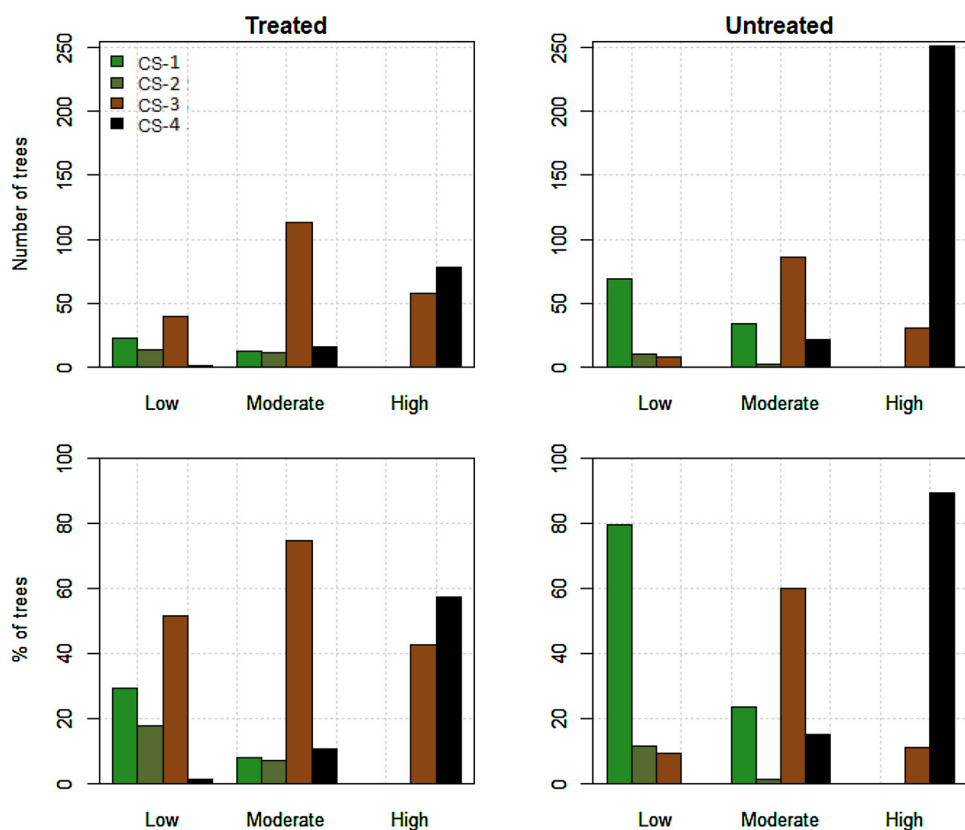
Fig. 2. Multiple bar plots of number of trees (upper) and percent of trees (bottom) in treated and untreated sites by low, moderate and high fire severity and crown severity (CS) classes (1–4). Crown severity classes are defined in Table 4. Fire severity is defined as low when live crowns predominate, as moderate when scorched crowns predominate, and as high when charred crowns predominate.

Table 6
Statistical summary of the imputed tree structural attributes.

Attributes	Treatment	Adj. R^2	RMSE		Bias	
			Absolute	Relative	Absolute	Relative
Ht (m)	All dataset	0.41	3.58	21.61	0.26	1.59
	Treated	0.37	3.62	21.55	0.15	0.91
	Untreated	0.44	3.71	22.70	0.35	2.16
CBH (m)	All dataset	0.11	4.88	59.91	0.16	2.02
	Treated	0.34	3.89	49.03	0.13	1.58
	Untreated	0.01	5.44	65.12	0.28	3.39
Live crown (%)	All dataset	0.35	32.55	172.40	−0.85	−4.50
	Treated	0.16	38.66	205.19	−1.74	−9.25
	Untreated	0.52	27.75	146.66	0.84	4.42
Scorched crown	All dataset	0.25	42.13	103.17	0.58	1.42
(%)	Treated	0.11	48.47	80.93	0.47	0.79
	Untreated	0.10	37.12	184.18	−0.19	−0.96
Charred crown	All dataset	0.52	33.57	83.34	0.27	0.66
(%)	Treated	0.26	35.98	169.26	1.26	5.96
	Untreated	0.56	31.19	51.20	−0.64	−1.05

Note: Ht: total height, CBH: crown base height.

The accuracy of CBH prediction when higher at the open-canopy treated plots than at the closed-canopy untreated plots (Figs. 5–7), with explained variation in CBH ranging from 5% to 25% (Table 8). ALS-derived height and intensity metrics were important in predicting CBH (Tables 7 and 8), while NDVI$_{MEAN}$ and EVI$_{MEAN}$ were also important predictors of CBH in the QB model. When ALS and QB derived metrics were combined, the percent variance explained in CBH models increased from 5% to 24%, but none of QB-derived metrics were retained in the model (Table 7 and 8).

The most important predictor metrics to explain the variation in BA$_T$ from ALS and ALS + QB models were height metrics, such as HMAX and HMEAN (Tables 7 and 8). BAI$_{MEAN}$ and RED were the most important predictors of BA$_T$ in the QB model, but the ALS and ALS + QB models performed better in untreated plots, whereas the QB model

performed better in treated plots (Figs. 5–7).

Random Forest models predicting BAL, BAS, and BAC from QB metrics alone were poor, and QB metrics did little to improve ALS + QB models. The selected predictors were similar for all the BA models weighted by crown color classes, where in general ALS intensity metrics were more important than QB metrics (Table 7). BA$_S$ is predicted more poorly than BA$_L$ or BA$_C$ (Table 8). BA$_L$ and BA$_C$ models performed better in untreated plots than treated plots (Table 8)..

Height and intensity metrics consistently exhibited high MIRs in all models (ALS, QB and ALS + QB models) and all study plots (treated and untreated). In the QB models, BAI, EVI, NDVI, and RED were better predictors of crown severity expressed in terms of weighted basal area (BA$_L$, BA$_S$, and BA$_C$) or as a class (CS 1–4) (Table 7). However, all models fitted to explain BA$_L$, BA$_S$, and BA$_C$ had a RMSE higher than 100%. The QB metrics did not improve the predictive models when included with ALS metrics (Table 8).

We developed additional Random Forest models for the two study areas to further investigate the potential of QB imagery collected either one or two years post fire (2008 and 2009) at Warm Lake and Secesh Meadows, respectively (see Supplementary Material - Tables S2 and S4). In the case of Warm Lake, the 2008 QB image was a better temporal match to the 2008 ALS and field data collection, thus providing a fairer comparison between the two sensor types (Table S2). On the other hand, for Secesh Meadows, 2009 QB model accuracies were relatively poorer, which matched expectations given the one-year difference with the ALS and field measures collected in 2008, one-year post fire (Table S4).

3.5.2. Crown Severity (CS) classification model

Moderate (ALS and ALS + QB) to weak (QB) classification accuracies were observed to model CS classes 1 to 4, based on the full dataset. As expected, noticeably higher accuracies were observed when using QB from 2008, the same year that the field and ALS data were collected (Table S3). Similarly to using QB from 2007 (Table 9), we
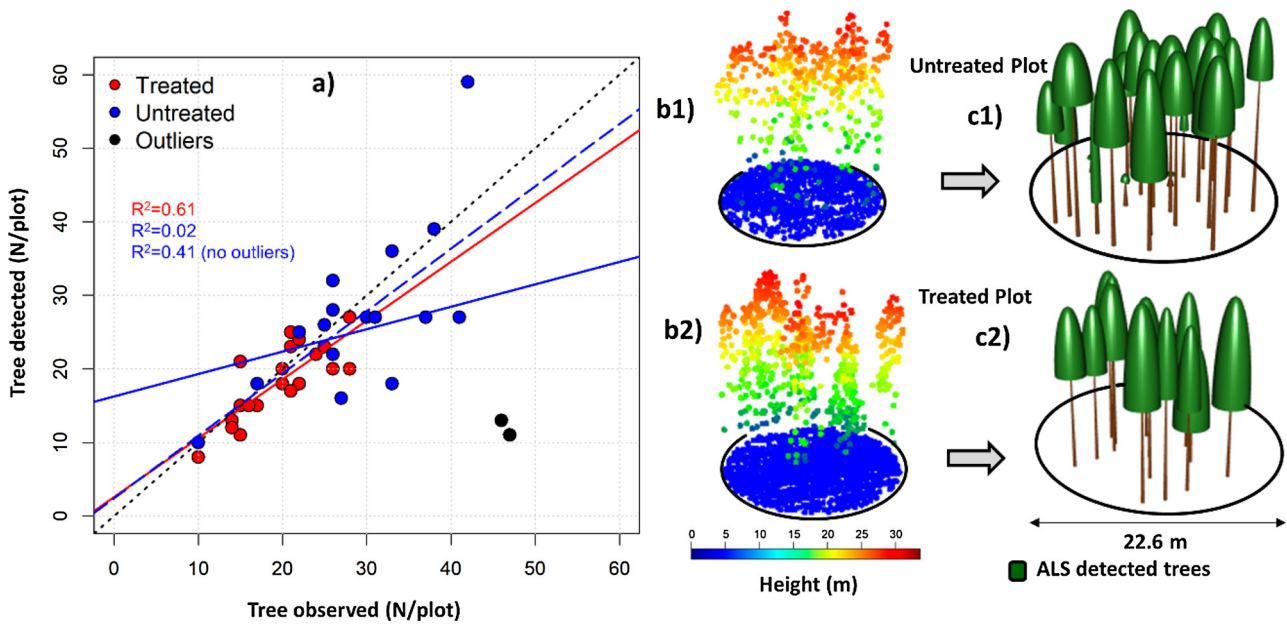
Fig. 3. Individual tree detection from ALS data. a) Number of trees detected by ALS in relation to number of trees observed; b1 and b2) ALS 3D point cloud of example plot colored by height, in a single treated/untreated example plot pair; c1 and c2) ALS 3D individual trees detected in the same example plot pair.

observed weaker classification accuracy when using QB from 2009 (Table S5). In general, classification model accuracies were better in untreated than treated areas (Table 9). Finally, CS-4 and CS-3 produced higher sensitivity values while CS-1 and CS-2 produced the higher

specificity values within the Random Forest classification models (Fig. 8).
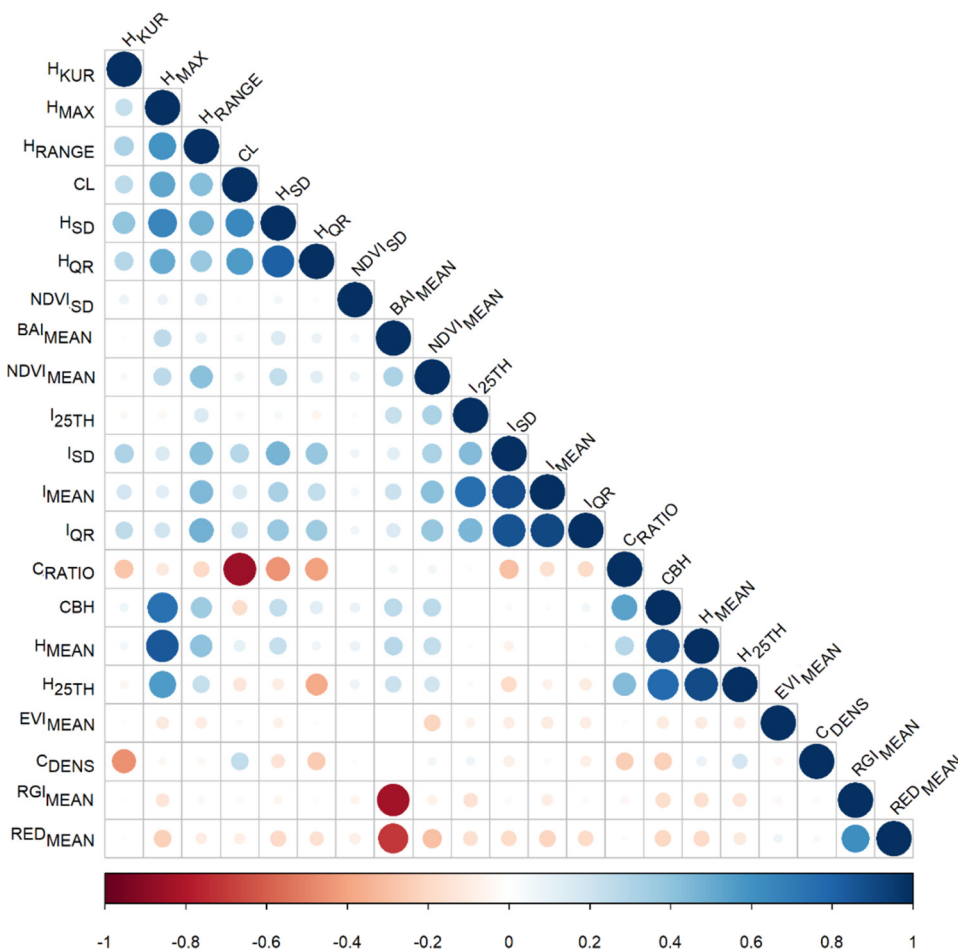
Fig. 4. Pearson correlations among ALS and QB metrics with a maximum allowable correlation of 0.9 for inclusion in the model improvement ratio (MIR) analysis. Positive correlations (r > 0) are displayed in blue and negative correlations (r < 0) in red. Strength of correlation is indicated by both the size of the circle and the color intensity as defined by the color ramp at the bottom. From the subset of 21 metrics included in the MIR analysis (Fig. 4), the most important explanatory variables for predicting the tree attributes and crown severity classes with Random Forest were selected based on higher values (MIR ≥ 0.35) (Table 7) (For interpretation of the references to colour in this figure legend, the reader is referred to the web version of this article).
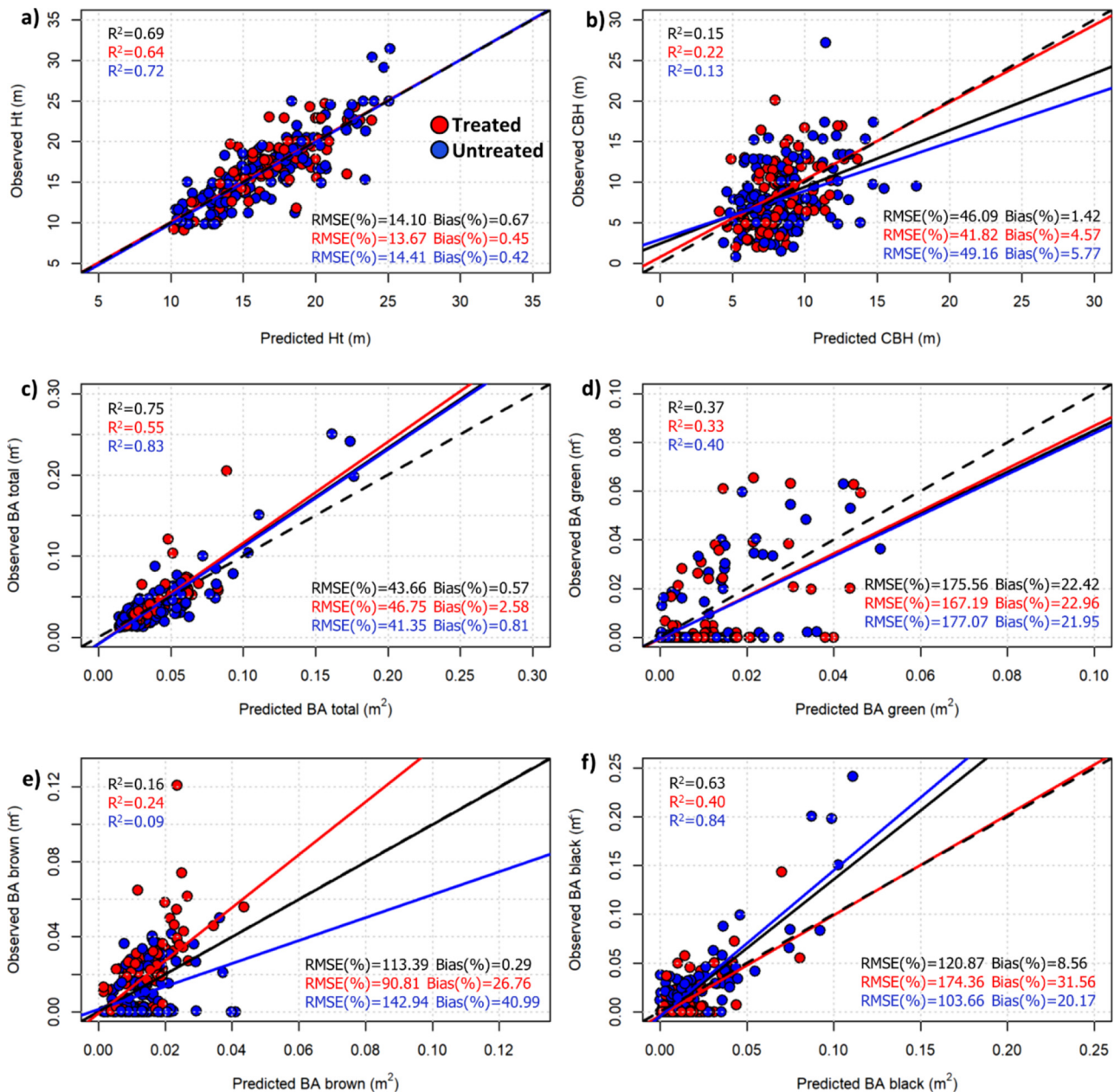
Fig. 5. Equivalence plots of the observed and the mean of predicted Ht (m) (**a**), CBH (m) (**b**), BA_T (m^2) (**c**), BA_L (m^2) (**d**), BA_S (m^2) (**e**), and BA_C (m^2) (**f**), obtained from the 500 bootstrapped Random Forest model runs using Airborne Laser Scanning (ALS) variables.

4. Discussion

Post-fire assessment is an essential activity for developing a management plan. Remote sensing adds value to field assessments as a way to expand information on damage level and its distribution over larger burned areas than can be practically surveyed in the field. However, most prior studies are not precisely characterizing fire effects because they only consider the three broad post-fire severity classes of low, moderate or high fire severity at the plot or stand level at a moderate spatial resolution of 30 m (e.g., Hudak et al., 2011b). Our study presents a novel approach for mapping post-fire charred, scorched, and live crowns at the tree level and may be the first to test both ALS and QB imagery at the tree level.

Spatial heterogeneity in fire severities of variable patch size mixed with unburned canopies are characteristic of large wildfires (Christensen, 1993; Turner et al., 1994; Broncano and Retana, 2004), the vast majority of which are much smaller than the East Zone and

Cascade Complex mega-fires that impacted our local study areas (Hudak et al., 2011a). The methodology presented herein based on ALS and QB data for individual tree detection, crown structure, and crown fire severity characterization in post-fire sites provides an alternative to the traditional area-based approach using moderate resolution Landsat satellite data. More resolute predictions of crown attributes (e.g., basal area, height, crown fire severity) can be aggregated into larger grid cells across the landscape for use in habitat models (Casas et al., 2016), whereas area-based predictions, if rescaled, may bias the habitat models (Garabedian et al., 2014). Moreover, burned severity patches are not homogeneously comprised of only low, moderate or high burn severity, but represent a mixture.

Individual tree approach may also minimize aggregation errors and allow land managers to more accurately identify severely burned areas (Montealegre et al., 2014). However, as fire severity increases, canopy fragmentation may occur, increasing the number of tree clumps (Montealegre et al., 2014) and making tree detection more difficult.
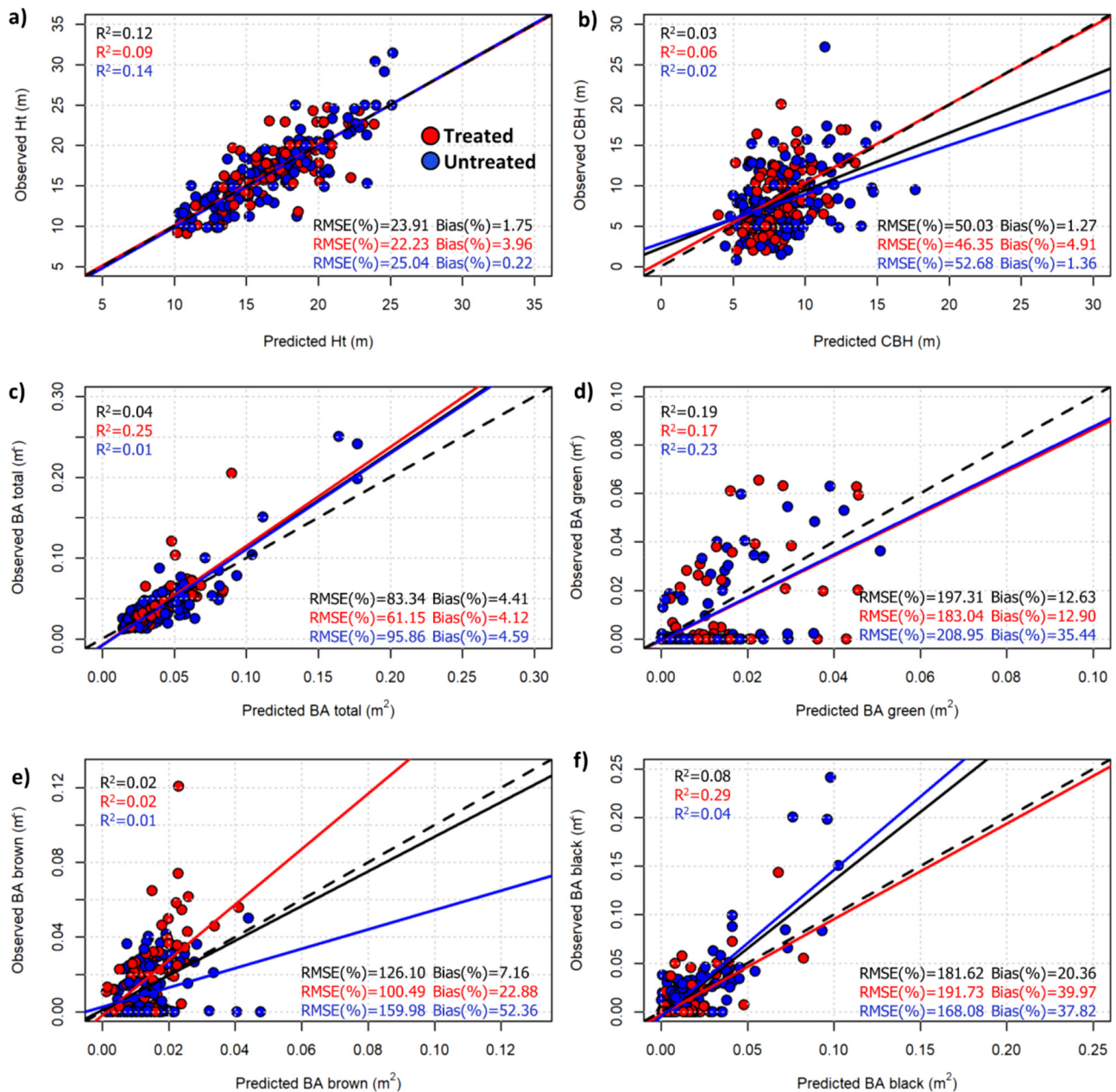
Fig. 6. Scatterplots of the observed and the mean of predicted Ht (m) (**a**), CBH (m) (**b**), BA_T (m^2) (**c**), BA_L (m^2) (**d**), BA_S (m^2) (**e**), and BA_C (**f**), obtained from the 500 bootstrapped Random Forest model runs using QuickBird (QB) variables.

Also, noise may be introduced into the tree detection by broken or partially consumed snags (Casas et al., 2016).

Immediately following high severity burns, overstory canopy is largely removed, but considerable overstory canopy remains after moderate or low severity burns (Lentile et al., 2006). By design, pre-fire fuel treatments dramatically reduce the tree density, creating open canopy conditions from what was previously closed canopy. Not surprisingly, we found better detection of individual trees in treated sites due to low canopy cover. In closed canopy conditions without a prior pre-fire treatment, individual tree detection was more difficult because of overlapping tree crowns of variable sizes, both live and dead (Wing et al., 2015). Previous studies also found higher tree detection accuracy in open canopy conditions (Casas et al., 2016; Falkowski et al., 2008; Silva et al., 2016). In two untreated plots that were the strongest outliers (i.e., highest numbers of trees detected, seen in close proximity in Fig. 3a), about three times as many trees were found from the ALS data as were tallied in the field. High fire severity occurred at these plots,

resulting in charred tree tops devoid of needles that offered very little surface area from which to reflect returns. We speculate that false detections may have been caused by larger branches than would be detected in an unburned, dense, closed canopy stand that still retained its needles, especially considering the lidar point density of 5 points m^{-2} was quite sparse by current standards. Additionally, leaning trees (i.e., trees bent at an angle $\geq 45°$ due to snow or other agents) probably contributed to false detections (Wing et al., 2015).

The main advantage of using r and MIR statistics for selecting the most important ALS and QB metrics was to achieve parsimonious models (Silva et al., 2017, 2017b). In this way, highly correlated metrics were removed, and the most important metrics were clearly identified. Herein, the chosen ALS height-related metrics (H_{MAX}, H_{MEAN}, H_{SD}, H_{RANGE} and H_{25TH}) were informative for characterizing forest structure attributes, such as Ht, CBH and BA. A notable result was that the chosen ALS intensity metrics, despite not having been normalized, were more informative for crown severity characterization (see Table 7)
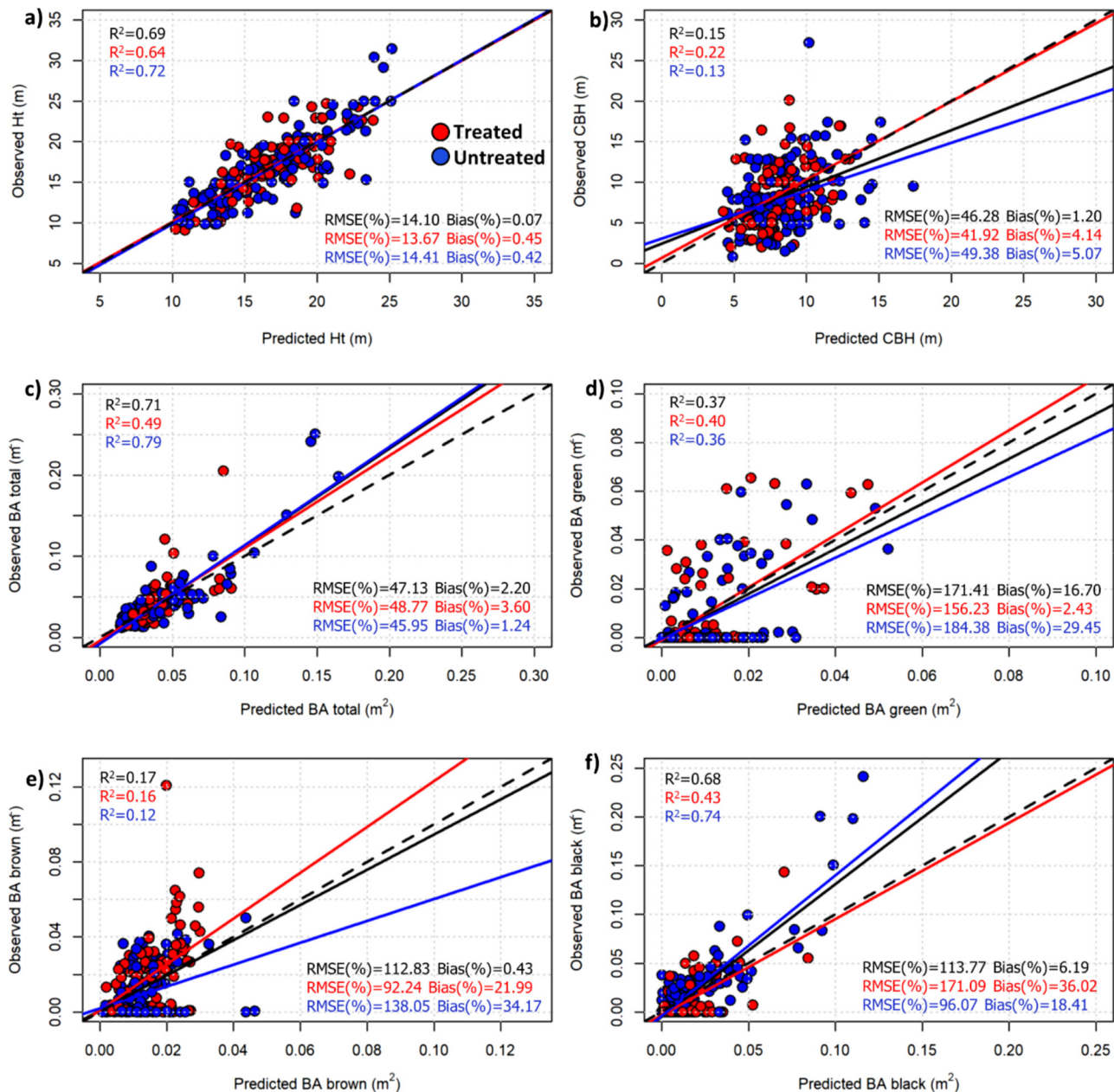
Fig. 7. Scatterplots of the observed and the mean of predicted Ht (m) (**a**), CBH (m) (**b**), BA_T (m^2) (**c**), BA_L (m^2) (**d**), BA_S (m^2) (**e**), and BA_C (m^2) (**f**), obtained from the 500 bootstrapped Random Forest model runs using Airborne Laser Scanning + Quickbird (ALS + QB) variables.

than the QB metrics. These intensity metrics include I_{MEAN}, I_{SD}, I_{QR} and I_{25TH}. The contribution of ALS intensity metrics to describe forest structure and distinguish fire severity classes found in this study agrees with other studies (e.g. Kim et al., 2009; Lim et al., 2003; Casas et al., 2016).

Random Forest regression and classification models produced better predictions of Ht, CBH, BA_{TL}, BA_L, BA_S, BA_C, and CS classes on untreated sites than treated sites. Also, in treated sites, the residual trees were more broadly and evenly spaced, whereas broken or partially consumed snags were common in untreated sites (Casas et al., 2016).

It is important to note that our study area had both treated and untreated sites that captured a broader fire severity gradient than would have either treatment condition alone. We observed differences in accuracy between ALS and QB models, both in treated and untreated areas. For instance, the prediction of Ht and CBH relied primarily on height-related metrics, mainly the H_{MAX} and H_{MEAN}, respectively. Other studies have attempted to predict CBH (Scott and Reinhardt, 2001)

because it is one of the most important forest structure attributes used in crown fire behavior models (Rothermel and Rinehart, 1983) and it is associated with tree fire severity. Because tree crown characteristics varied so dramatically due to their fire severity condition, CBH predicted in our study had a larger RMSE than previous studies. For instance, Vauhkonen (2010) using ALS data estimated CBH with a RMSE varying between 1.54–3.88 m, while Jung et al. (2011) had a lower RMSE of 1.87. In both studies, the study areas were unburned forests, whereas our case study area had both treatment and wildfire effects contributing to the variation.

Other studies have shown that BA_T, as well as live BA and dead BA (Bright et al., 2013, 2014), may be reasonably predicted from height-related metrics. Hudak et al. (2006) estimated BA_T of an actively managed mixed forest in Idaho, USA using ALS and Advanced Land Imager (ALI) multispectral satellite data. They also explained more variance (ranging from R^2 = 0.71 to R^2 = 0.89) using ALS data alone or in combination with ALI spectral indices than using ALI metrics alone.

Table 7

Airborne Laser Scanning (ALS) and QuickBird (QB) metrics selected as important for predicting the response variables, according to the model improvement ratio (MIR) value (MIR ≥ 0.35).

Explanatory Variables		Response Variables						
		Ht (m)	CBH (m)	BA_T (m^2)	BAL (m^2)	BAS (m^2)	BAC (m^2)	Crown Fire Severity Classes
ALS	H_{MAX}	1.00	1.00	1.00	1.00	0.49	1.00	0.39
	H_{MEAN}	0.35	0.85	0.65	0.65	0.39	0.42	0.56
	H_{SD}		0.37		0.87	0.68		
	H_{QR}							
	H_{RANGE}				0.85	0.73		0.93
	H_{25TH}		0.49			0.44		0.37
	H_{KUR}							
	CL				0.36		0.40	
	CBH		0.55	0.35	0.38	0.44		
	C_{RATIO}							
	C_{DENS}							
	I_{SD}		0.44		0.48	1.00	0.39	0.56
	I_{MEAN}		0.50		0.65	0.57	0.65	0.96
	I_{QR}		0.50		0.89	0.44	0.38	0.99
	I_{25TH}		0.45		0.42		0.70	0.96
QB	$NDVI_{MEAN}$	0.71	1.00	0.47	1.00	0.61	0.79	1.00
	$NDVI_{SD}$	0.59	0.66		0.41	0.36	0.43	0.68
	EVI_{MEAN}	0.67	0.95	0.39	0.86	0.59	0.61	0.89
	BAI_{MEAN}	0.96	0.94	0.99	0.62	1.00	0.89	0.56
	RGI_{MEAN}	0.86	0.75	0.50	0.54	0.43	0.70	0.57
	RED_{MEAN}	1.00	0.94	0.98	0.69	0.83	1.00	0.57
ALS + QB	H_{MAX}	1.00	1.00	1.00	0.87	0.40	1.00	0.39
	H_{MEAN}	0.35	0.85	0.64	0.44		0.37	
	H_{SD}					0.72		
	H_{QR}							
	H_{RANGE}				0.62	0.92		0.50
	H_{25TH}		0.46					
	H_{KUR}							
	CL						0.36	
	CBH		0.50					
	C_{RATIO}							
	C_{DENS}							
	I_{SD}		0.37			0.96		0.50
	I_{MEAN}		0.45			0.52	0.53	0.69
	I_{QR}		0.44		0.46	0.42		0.68
	I_{25TH}		0.43				0.58	0.59
	$NDVI_{MEAN}$				1.00	0.50		1.00
	$NDVI_{SD}$							0.44
	EVI_{MEAN}				0.48			0.68
	BAI_{MEAN}					0.39		
	RGI_{MEAN}							
	RED_{MEAN}					0.36		

Note: MIR values range from 0 to 1, where 1 indicates most important.

Table 8

Accuracies of Random Forest (RF) models in terms of Adj.R^2, Root Mean Square Error (RMSE) and Bias calculated by the relationship between predicted and observed tree structural attributes. ALS: Airborne Laser Scanning (2008), QB: QuickBird imagery (2007).

	Attributes	Crown Metrics	Adj. R^2	RMSE		Bias	
				Absolute	Relative	Absolute	Relative
ALS	Ht	H_{MAX}, H_{MEAN}	0.66	2.38	14.47	-2.50×10^{-2}	0.15
	CBH	CBH, H_{25TH}, H_{MAX}, H_{MEAN}, H_{SD}, I_{25TH}, I_{QR}, I_{MAX}, I_{MEAN}	0.25	3.58	43.07	2.43×10^{-2}	0.29
	BA_T	CBH, CL, H_{MAX}, H_{MEAN}	0.55	1.86×10^{-2}	50.31	-2.70×10^{-4}	-0.75
	BA_L	CBH, H_{MAX}, H_{MEAN}, H_{RANGE}, I_{25TH}, I_{QR}, I_{SD}, I_{MEAN}	0.46	1.21×10^{-2}	155.89	1.21×10^{-4}	1.56
	BA_S	CBH, H_{25TH}, H_{MAX}, H_{MEAN}, H_{RANGE}, H_{SD}, I_{QR}, I_{SD}, I_{MEAN}	0.06	1.80×10^{-2}	134.60	2.82×10^{-4}	2.07
	BA_C	CL, H_{MAX}, H_{MEAN}, I_{25TH}, I_{MEAN}	0.63	1.69×10^{-2}	107.03	1.48×10^{-4}	0.94
QB	Ht	BAI_{MEAN}, EVI_{MEAN}, $NDVI_{MEAN}$, $NDVI_{SD}$, RED_{MEAN}, RGI_{MEAN}	0.12	4.00	23.90	-0.29	-1.75
	CBH	BAI_{MEAN}, EVI_{MEAN}, $NDVI_{MEAN}$, $NDVI_{SD}$, RED_{MEAN}, RGI_{MEAN}	0.05	4.08	49.20	3.00×10^{-2}	0.36
	BA_T	BAI_{MEAN}, EVI_{MEAN}, $NDVI_{MEAN}$, RED_{MEAN}, RGI_{MEAN}	0.03	2.80×10^{-2}	76.50	6.20×10^{-4}	1.68
	BA_L	BAI_{MEAN}, EVI_{MEAN}, $NDVI_{MEAN}$, $NDVI_{SD}$, RED_{MEAN}, RGI_{MEAN}	0.30	1.40×10^{-2}	178.00	9.70×10^{-5}	1.25
	BA_S	BAI_{MEAN}, EVI_{MEAN}, $NDVI_{MEAN}$, $NDVI_{SD}$, RED_{MEAN}, RGI_{MEAN}	0.03	1.80×10^{-2}	138.00	3.80×10^{-4}	2.82
	BA_C	BAI_{MEAN}, EVI_{MEAN}, $NDVI_{MEAN}$, $NDVI_{SD}$, RED_{MEAN}, RGI_{MEAN}	0.24	2.40×10^{-2}	152.00	6.70×10^{-4}	4.24
ALS + QB	Ht	H_{MAX}, H_{MEAN}	0.66	2.39	14.52	-1.99×10^{-2}	-0.12
	CBH	CBH, H_{25TH}, H_{MAX}, H_{MEAN}, I_{25TH}, I_{QR}, I_{MEAN}, I_{SD}	0.24	3.61	43.49	2.45×10^{-2}	0.30
	BA_T	H_{MAX}, H_{MEAN}	0.52	1.95×10^{-2}	52.57	-1.43×10^{-4}	-0.39
	BA_L	H_{MEAN}, H_{MAX}, H_{MEAN}, H_{RANGE}, I_{QR}, EVI_{MEAN}, $NDVI_{MEAN}$	0.49	0.01	151.14	1.22×10^{-4}	1.57
	BA_S	H_{MAX}, H_{RANGE}, H_{SD}, I_{QR}, I_{MEAN}, I_{SD}, BAI_{MEAN}, RED_{MEAN}, $NDVI_{MEAN}$	0.12	1.76×10^{-2}	129.43	3.34×10^{-4}	2.45
	BA_C	CL, H_{MAX}, H_{MEAN}, I_{25TH}, I_{MEAN}	0.62	0.02	107.26	1.12×10^{-4}	0.71

Table 9

Accuracies of Random Forest (RF) models – to classify crown severity (CS – 1–4) in terms of Accuracy and Kappa attributes calculated by the relationship between predicted and observed attributes.

N	Condition	Crown Metrics	Kappa	Accuracy (%)
ALS	All dataset	H_{25TH}, H_{MAX}, H_{MEAN}, H_{RANGE}, I_{25TH}, I_{QR}, I_{SD}, I_{MEAN}	0.456	65.76
	Treated	CBH, C_{DENS}, H_{MAX}, H_{RANGE}, H_{SD}, I_{25TH}, I_{MEAN}, I_{SD}	0.280	60.79
	Untreated	H_{25TH}, H_{MEAN}, H_{RANGE}, I_{25TH}, I_{QR}, I_{MEAN}, I_{SD}	0.539	74.55
QB	All dataset	BAI_{MEAN}, EVI_{MEAN}, $NDVI_{MEAN}$, $NDVI_{SD}$, RED_{MEAN}, RGI_{MEAN}	0.393	61.24
	Treated	BAI_{MEAN}, EVI_{MEAN}, $NDVI_{MEAN}$, $NDVI_{SD}$, RED_{MEAN}, RGI_{MEAN}	0.283	60.79
	Untreated	e EVI_{MEAN}, $NDVI_{MEAN}$, RGI_{MEAN}	0.474	70.18
ALS + QB	All dataset	EVI_{MEAN}, H_{KUR}, H_{MAX}, H_{RANGE}, I_{25TH}, I_{QR}, I_{SD}, I_{MEAN}, $NDVI_{MEAN}$, $NDVI_{SD}$	0.463	65.91
	Treated	CBH, C_{DENS}, H_{MAX}, H_{RANGE}, H_{SD}, I_{25TH}, I_{MEAN}, I_{SD}, BAI_{MEAN}, EVI_{MEAN}, $NDVI_{MEAN}$, $NDVI_{SD}$, RED_{MEAN}, RGI_{MEAN}	0.379	66.91
	Untreated	H_{RANGE}, I_{25TH}, I_{QR}, I_{MEAN}, I_{SD}, EVI_{MEAN}, $NDVI_{MEAN}$, $NDVI_{SD}$	0.542	74.56
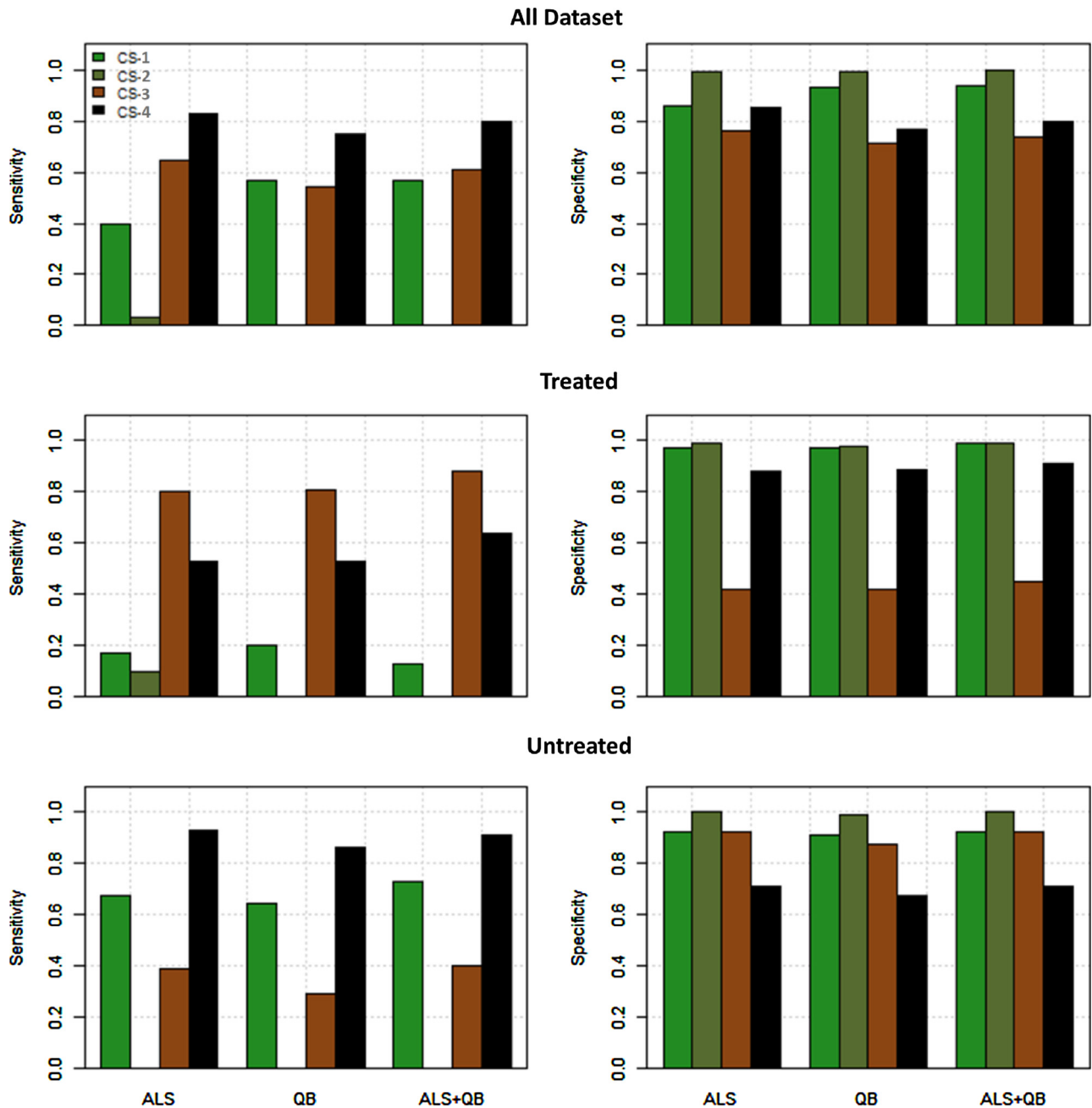
Fig. 8. Sensitivity (%) (left) and specificity (%) (right) from the Random Forest (RF) classification models for crown severity (CS) classes 1–4 (see Table 1 for definitions).

In this study, vegetation index derived from QB-derived suite of metrics (e.g. NDVI$_{MEAN}$, BAI$_{MEAN}$ and RED$_{MEAN}$) produced the highest MIR for predicting basal area weighted by crown severity (live, scorched and charred) and the CS classes. NDVI is a useful indicator of photosynthetic capacity (Willis, 2015) but also is affected by understory and soil properties that contribute to background reflectance (Escuin et al., 2008), which varies greatly between burn severity classes. A reasonable and significant correlation between NDVI and fire severity was found by Diaz-Delgado et al. (2003). On the other hand, Oliveras et al. (2009) and Hammill and Bradstock (2006) found low correspondence between NDVI and percentage of charred or live canopies.

While height-related metrics from ALS may be most useful for predicting and mapping forest structural attributes (e.g., Ht, CBH, and BA$_T$), increased availability of high resolution imagery and/or ALS intensity metrics are improving post-fire CS classification (Kim et al., 2009). Intensity and spectral information about post-fire disturbance were the most important predictors for all the response variables related to crown condition (live, scorched, and charred) in this study (see Table 7). We can highlight all selected intensity metrics and the QB indices derived from the red and NIR bands (NDVI, EVI, BAI, and RED), which had relatively higher importance in the predicted models. ALS intensity metrics alone were selected to predict BA$_L$ and BA$_C$ and CS classes (Tables 7–9). This may be attributable to higher near-infrared return intensity reflected from green rather than non-photosynthetic vegetation components. Moreover, ALS intensity can be used to estimate and distinguish between live and dead biomass (Kim et al., 2009), which our results support (Fig. S1).

When both ALS and QB metrics were combined, NDVI$_{MEAN}$ was the most important explanatory variable to predict BAL. The same was not observed for predicting BAC where none of the QB-derived indices was important. Using only ALS data, H$_{MAX}$ was the most important explanatory variable for both BA$_L$ and BA$_C$, as well as BA$_T$. A second explanatory variable for predicting BA$_L$ and BA$_C$ according to MIR was I$_{QR}$ and I$_{25TH}$, respectively. Higher ALS intensities are associated with green foliage, while lower ALS intensities are associated with black vegetation (Fig. S1). Kim et al. (2009) used ALS data to distinguish between live and dead standing tree biomass in Grand Canyon National Park, USA, and Bright et al. (2013) considered ALS intensity metrics to predict both live and dead BA in western coniferous forests impacted by bark beetles. These studies associated low intensity returns with dead biomass, finding that the low intensity ALS returns were sensitive to the proportion of echoes from non-photosynthetic woody material, including dead trees.

The accuracy of BA$_S$ models was improved 12% when ALS and QB metrics were combined (Table 8). The brown color of dead or dying needles may be associated with pests and diseases, as well as needles scorched by fire. Coops et al. (2006) used QB imagery to detect red attack damage due to mountain pine beetle infestation, and they found RGI to be a good index to discriminate red attack crowns from non-attack. Unlike Coops et al. (2006), among the QB metrics in our study, BAI, NDVI and RED were selected as having higher importance than RGI to predict BA$_S$. More generally, however, ALS metrics were more important than QB metrics as explanatory variables to predict BA$_S$. Part of the issue is that as the post-fire scene changes, so will its reflectance properties. Scorched needles falling from the trees in the days, weeks, and months following a fire would explain our generally poorer ability to predict BA$_S$ compared to BA$_L$ and BA$_C$ (Table 8), and crown severity class 3 compared to crown severity classes 1, 2, or 4 (Table 9).

Random Forest models for classifying CS produced satisfactory accuracy. ALS intensity metrics were important to predict CS class in the absence of QB metrics. The 2-year post-fire QB at Secesh Meadows diminished the utility of QB data for postfire tree crown assessment (Tables S3–S4), relative to the 1-year post-fire QB at Warm Lake (Tables S1–S2). The post-fire scene changes quickly during the first post-fire year, and then the rate of change as site recovery slows over time (Lewis et al., 2017). Among the ALS intensity metrics, I$_{QR}$, H$_{RANGE}$ and I$_{25TH}$

where the most important to predict BA$_L$, BA$_S$, BA$_C$, respectively. Complex associations between wildfire effects and fuel conditions can cause, for instance, mixed live and charred crowns, while scorched crowns necessarily fall within the gradient from unburned or low to high severity conditions (Jain and Graham, 2007). Few studies have attempted to map crown severity class at fine-scales in a post-fire forest using field or remote sensing (e.g. Jain and Graham, 2007); and most existing studies using either ALS or QB are focused on snag detection (e.g. Jain and Graham, 2007; Casas et al., 2016; Vogeler et al., 2016) instead of crown condition.

Fuel treatments produced a diverse set of tree severity outcomes compared to the untreated stands. It is not surprising that the treated sites tended to have more scorched trees crowns compared to the untreated sites (Fig. 2). However, there were fewer fully consumed crowns (charred crowns) in the treated sites (approximately 60% compared to the untreated stands that contained close to 100% of some trees totally charred); thus, the treatments did diminish the amount of crown fire. Graham et al. (2009) noted that in the Warm Lake Wildfire Complex there were multiple head fires that burned into and around the treated sites.

5. Conclusion

In this study, we used tree measurements collected in 40 field plots to characterize fire effects on individual tree crowns and then summarized at the plot level. Our study shows the greater utility of ALS data compared to high resolution QB imagery for estimating post-fire scorched and charred tree crowns, basal area, tree height and crown base height in a mixed conifer forest from one-year post-fire ALS and either immediate, one-year or two-year post-fire multispectral QB images of high resolution. ALS-derived models performed better than QB imagery for characterizing both tree structure attributes and crown severity, but the combination of ALS and QB derived metrics slightly improved the accuracy of only a few models. We hope that the promising results for characterizing post-fire crown attributes in this study will stimulate further research and applications worldwide. Future research and development could attempt to automate and apply such models across broader spatial extents to generate stem maps across burned landscapes to greatly assist forest managers in the preparation of conservation and restoration plans after wildfires, and for wildlife habitat assessments and other post-fire applications.

Appendix A. Supplementary data

Supplementary material related to this article can be found, in the online version, at doi:https://doi.org/10.1016/j.ecolmodel.2019.108820.

References

Agca, M., Popescu, S.C., Harper, C.W., 2011. Deriving forest canopy fuel parameters for loblolly pine forests in eastern Texas. Can. J. For. Res. 41, 1618–1625.

Agee, J.K.S., Carl, N., 2005. Basic principles of forest fuel reduction treatments. For. Ecol. Manage. 211, 83–96.

Andersen, H.E., McGaughey, R.J., Reutebuch, S.E., 2005. Estimating forest canopy fuel parameters using LIDAR data. Remote Sens. Environ. 94, 441–449.

Aurenhammer, F., 1991. Voronoi diagrams—a survey of a fundamental geometric data

structure. ACM Comp. Surv. 23, 345–405.
Barton, I., Géza, K., Kornél, C., Markus, H., Norbert, P., 2017. Treefall gap mapping using sentinel-2 images. Forests 8, 426. https://doi.org/10.3390/f8110426.
Benaglia, T., Chauveau, D., Hunter, D., Young, D., 2009. Mixtools: an R package for analyzing finite mixture models. J. Stat. Softw. 32, 1–29 University of California, Los Angeles.
Breiman, L., 2001. Random forests. Mach. Learn. 45, 5–32.
Bright, B.C., Hicke, J.A., Hudak, A.T., 2012. Estimating aboveground carbon stocks of a forest affected by mountain pine beetle in Idaho using lidar and multispectral imagery. Remote Sens. Environ. 124, 270–281.
Bright, B.C., Hudak, A.T., McGaughey, R., Andersen, H.E., Negron, J., 2013. Predicting live and dead tree basal area of bark beetle-affected forests from discrete-return lidar. Can. J. Remote. Sens. 39 (S1), S99–S111.
Bright, B.C., Hudak, A.T., Kennedy, R.E., Meddens, A.J.H., 2014. Landsat time series and lidar as predictors of live and dead basal area across five bark beetle-affected forests. IEEE J. Sel. Top. Appl. Earth Obs. Remote. Sens. 7 (8), 3440–3452. https://doi.org/10.1109/JSTARS.2014.2346955.
Broncano, M.J., Retana, J., 2004. Topography and pre-fire vegetation affecting the spatial heterogeneity generated after a large forest wildfire in the Mediterranean Basin. Int. J. Wildland Fire 13, 209–216. https://doi.org/10.1071/WF03036.
Casas, A., García, M., Rodney, B., Koltunov, A., Ramírez, C., Ustin, S., 2016. Burned forest characterization at single-tree level with airborne laser scanning for assessing wildlife habitat. Remote Sens. Environ. 175, 231–241.
Christensen, N.L., 1993. Fire regimes and ecosystems dynamics. In: Crutzen, P.J., Goldammer, J.G. (Eds.), In 'Fire in the Environment: Ecological, Atmospheric and Climatic Importance of Vegetation Fires'. Wiley, New York, pp. 233–244.
Chuvieco, E., 2002. Teledetección Ambiental. La Observación de la Tierra desde el Espacio.' (Ariel Ciencia: Barcelona).
Cohen, J.D., 2000. Preventing disaster: home ignitability in the wildland-urban interface. J. For. 98 (3), 15–21.
Coops, N.C., Johnson, M., Wulder, M., White, J., 2006. Assessment of QuickBird high spatial resolution imagery to detect red attack damage due to mountain pine beetle infestation. Remote Sens. Environ. 103 (1), 67–80 15 July.
Coren, F., Sterzai, P., 2006. Radiometric correction in laser scanning. Int. J. Remote Sens. 27 (15–16), 3097–3104.
Crookston, N.L., Finley, A.O., 2008. yaImpute an R package for kNN imputation. J. Stat. Softw. 23, 1–16.
Dalponte, M., 2018. Fusion of hyperspectral and LIDAR remote sensing data for classification of complex forest areas. Geosci. Remote Sens. 46, 1416–1427.
Davranche, A., Lefebvre, G., Poulin, B., 2010. Wetland monitoring using classification trees and SPOT-5 seasonal time series. Remote Sens. Environ. 114, 552–562.
Diaz-Delgado, R., Loret, F., Pons, X., 2003. Influence of fire severity on plant regeneration by means of remote sensing imagery. Int. J. Remote Sens. 24 (8), 1751–1763.
Ellison, A., Moseley, C., Bixler, R.P., 2015. Drivers of Wildfire Suppression Costs Literature Review and Annotated Bibliography. Oregon, USA. 40p.. .
Escuin, S., Navarro, R., Fernandez, P., 2008. Fire severity assessment by using NBR (normalized burn ratio) and NDVI (normalized difference vegetation index) derived from LANDSAT TM/ETM images. Int. J. Remote Sens. 29, 1053–1073. https://doi.org/10.1080/01431160701281072.
ESRI, 2011. ArcGIS Desktop: Release 10. Environmental Systems Research Institute, Redlands, CA.
Evans, J.S., Cushman, S.A., 2009. Gradient modeling of conifer species using Random Forests. Landsc. Ecol. 5, 673–683.
Evans, J.S., Murphy, M.A., Holden, Z.A., Cushman, S.A., 2010. Modeling species distribution and change using random forests. In: Drew, C.A., Huettmann, F., Wiersma, Y. (Eds.), Predictive Modeling in Landscape Ecology. Springer, New York, NY, USA, pp. 139–159.
Evans, J.S., 2018. rfUtilities: Random Forests Model Selection and Performance Evaluation, Version 2.1-3. Accessed Oct. 15 2018,. https://cran.r-project.org/web/packages/rfUtilities/index.html.
Falkowski, M.J., Smith, A.M.S., Gessler, P.E., Hudak, A.T., Vierling, L.A., Evans, J.S., 2008. The influence of conifer forest canopy cover on the accuracy of two individual tree measurement algorithms using LiDAR data. Can. J. Remote. Sens. 34 (S2), S338–S350.
French, N.H.F., Kasischke, Hall, E.S., Murphy, K.A., Verbyla, D.L., Hoy, E.E., 2008. Using landsat data to assess fire and burn severity in the North American Boreal Forest Region: an overview and summary of results. Int. J. Wildland Fire 17, 443–462 2008.
Garabedian, J.E., McGaughey, R.J., Reutebuch, S.E., Parresol, B.R., Kilgo, J.C., Moorman, C.E., Peterson, M.N., 2014. PetersonQuantitative analysis of woodpecker habitat using high-resolution airborne lidar estimates of forest structure and composition. Remote Sens. Environ. 145, 68–80.
Goetz, S.J., Steinberg, D., Betts, M.G., Holmes, R.T., Doran, P.J., Dubayah, R., Hofton, M., 2010. Lidar remote sensing variables predict breeding habitat of a Neotropical migrant bird. Ecology 91, 1569–1576.
Graham, R.T., Jain, T.B., Loseke, M., 2009. Fuel treatments, fire suppression, and their interaction with wildfire and its impacts: the warm Lake experience during the Cascade complex of wildfires in central Idaho, 2007. Gen. Tech. Rep. RMRS-GTR-229. U.S. Department of Agriculture, Forest Service, Rocky Mountain Research Station, Fort Collins, CO 36 p.
Graham, R.T., McCaffrey, S., Theresa, B., 2004. Science basis for changing forest structure to modify wildfire behavior and severity. Gen. Tech. Rep. RMRS-GTR-120. Rocky Mountain Research Station, USDA Forest Service, Fort Collins, CO 43 p.
Hammill, K.A., Bradstock, R.A., 2006. Remote sensing of fire severity in the Blue Mountains: influence of vegetation type and inferring fire intensity. Int. J. Wildland Fire 15, 213–226. https://doi.org/10.1071/WF05051.
Hart, S.J., Veblen, T.T., 2015. Detection of spruce beetle-induced tree mortality using

high- and medium-resolution remotely sensed imagery. Remote Sens. Environ. 168, 134–145.
Holden, Z.A., Morgan, P., Smith, A.M.S., Vierling, L., 2010. Beyond Landsat: a comparison of four satellite sensors for detecting burn severity in ponderosa pine forests of the Gila Wilderness, NM, USA. Int. J. Wildland Fire 19, 449–458.
Holden, Z.A., Luce, C.H., Crimmins, M.A., Morgan, P., 2012. Wildfire extent and severity correlated with annual streamflow distribution and timing in the Pacific Northwest, USA (1984–2005). Ecohydrology 5, 677–684.
Hollander, M., Wolfe, D.A., 1973. Nonparametric Statistical Inference. John Wiley & Sons, New York, pp. 68–75.
Hurteau, M.D., North, M., 2010. Carbon recovery rates following different wildfire risk mitigation treatments. For. Ecol. Manage. 260, 930–937.
Hudak, A.T., Crookston, N.L., Evans, J.S., Falkowski, M.J., Smith, A.M., Gessler, P.E., Morgan, P., 2006. Regression modeling and mapping of coniferous forest basal area and tree density from discrete-return lidar and multispectral satellite data. Can. J. Remote. Sens. 32 (2), 126–138 2006.
Hudak, A.T., Morgan, P., Bobbitt, M.J., Smith, A.M.S., Lewis, S.A., Lentile, L.B., Robichaud, P.R., Clark, J.T., McKinley, R.A., 2007. The relationship of multispectral satellite imagery to immediate fire effects. Fire Ecol. 3, 64–90.
Hudak, A.T., Crookston, N.L., Evans, J.S., Hall, D.E., Falkowski, M.J., 2008. Nearest neighbor imputation of species-level, plot-scale forest structure attributes from lidar data. Remote Sens. Environ. 112, 2232–2245.
Hudak, A.T., Evans, J.S., Smith, A.M.S., 2009. Review: LiDAR utility for natural resource managers. Remote Sens. 1, 934–951.
Hudak, A.T., Rickert, I., Morgan, P., Strand, E., Lewis, S.A., Robichaud, P.R., Hoffman, C., Zachary, A., 2011a. Review of fuel treatment effectiveness in forests and rangelands and a case study from the 2007 megafires in central, Idaho, USA. Gen. Tech. Rep. RMRS-GTR-252. U.S. Department of Agriculture, Forest Service, Rocky Mountain Research Station, Fort Collins, CO 60 p.
Hudak, A.T., Jain, T.B., Morgan, P., Clark, J.T., 2011b. Remote sensing of WUI fuel treatment effectiveness following the 2007 wildfires in central Idaho. In: Wade, D.D., Robinson, M.L. (Eds.), Proceedings of the 3rd Fire Behavior and Fuels Conference, October 25-29, 2010. Spokane, WA. Birmingham, AL: International Association of Wildland Fire. 11 p.
Huete, A., Didan, K., Miura, T., Rodriguez, E.P., Gao, X., Ferreira, L.G., 2002. Overview of the radiometric and biophysical performance of the MODIS vegetation indices. Remote Sens. Environ. 83, 195–213.
Huete, A.R., 1988. A soil-adjusted vegetation index (SAVI). Remote Sens. Environ. 25, 295–309.
Ice, G.G., Neary, D.G., Adams, P.W., 2004. Effects of wildfire on soils and watershed processes. J. For. 102 (6), 16–20.
Isenburg, M., 2018. LAStools—Efficient Tools for Lidar Processing. Available online: http://www.cs.unc.edu/~isenburg/lastools/ (accessed on 3 January 2018). .
Jain, T.B., Graham, R.T., 2007. The relation between tree burn severity and Forest structure in the Rocky mountains. USDA Forest Service Gen. Tech. Rep. PSW-GTR-203. 2007. https://www.fs.fed.us/psw/publications/documents/psw_gtr203/psw_gtr203_017jain.pdf.
Jung, S.E., Kwak, D.A., Park, T., Lee, W.K., Yoo, S., 2011. Estimating crown variables of individual trees using airborne and terrestrial laser scanners. Remote Sens. 3, 2346–2363. https://doi.org/10.3390/rs3112346.
Kane, V.R., Lutz, J.A., Roberts, S.L., Smith, D.F., McGaughey, R.J., Povak, N.A., Brooks, M.L., 2013. Landscape-scale effects of fire severity on mixed-conifer and red fir forest structure in Yosemite National Park. For. Ecol. Manage. 287, 17–31.
Keeley, J., 2009. Fire intensity, fire severity and burn. Int. J. Wildland Fire 18 (1), 116–126. https://doi.org/10.1071/WF07049.
Kim, Y., Yang, Z., Warren, B., Pflugmacher, D., Lauver, L., Vankat, J.L., 2009. Distinguishing between live and dead standing tree biomass on the North Rim of Grand Canyon National Park, USA using small-footprint lidar data. Remote Sens. Environ. 113 (11), 2499–2510.
Kokaly, R.F., Rockwell, B.W., Haire, S.L., King, T.V.V., 2007. Characterization of post-fire surface cover, soils, and burn severity at the Cerro Grande Fire, New Mexico, using hyperspectral and multispectral remote sensing. Remote Sens. Environ. 106 (3), 305–325.
Kukko, A., Kaasalainen, S., Litkey, P., 2008. Effect of incidence angle on laser scanner intensity and surface data. Appl. Opt. 47https://doi.org/10.1364/AO.47.000986. p. 986.
Lentile, L.B., Holden, Z.A., Smith, A.M.S., Falkowski, M.J., Hudak, A.T., Morgan, P., Lewis, S.A., Gessler, P.E., Benson, N.C., 2006. Remote sensing techniques to assess active fire characteristics and post-fire effects. Int. J. Wildland Fire 15, 319–345.
Lewis, S.A., Hudak, A.T., Robichaud, P.R., Morgan, P., Satterberg, K.L., Strand, E.K., Smith, A.M.S., Zamudio, J.A., Lentile, L.B., 2017. Indicators of burn severity and ecosystem response in mixed conifer forests of western Montana. Int. J. Wildland Fire 26, 755–771. https://doi.org/10.1071/WF17019.
Liaw, A., Wiener, M., 2015. RandomForest: Breiman and Cutler's Random Forests for Classification and Regression, Version 4.6–12. Available online: https://cran.rproject.org/web/packages/randomForest/ (Accessed on 15 August 2017). .
Lim, K., Treitz, P., Baldwin, K., Morrison, I., Green, J., 2003. Lidar remote sensing of biophysical properties of tolerant northern hardwood forests. Can. J. Remote. Sens. 29 (5), 658–678.
Maltamo, M., Malinen, J., Packalén, P., Suvanto, A., Kangas, J., 2006. Nonparametric estimation of stem volume using airborne laser scanning, airborne photography, and stand-register data. Can. J. For. Res. 36 (2), 426–436.
Martinuzzi, S., Vierling, L.A., Gould, W.A., Falkowski, M.J., Evans, J.S., Hudak, A.T., 2009. Mapping snags and understory shrubs for a Lidar-based assessment of wildlife habitat suitability. Remote Sens. Environ. 113, 2522–2546.
McCarley, T.R., Kolden, C.A., Vaillant, N.M., Hudak, A.T., Smith, A.M.S., Wing, B.M.,

Kellogg, B.S., Kreitler, J., 2017. Multi-temporal LiDAR and Landsat quantification of fire-induced changes to forest structure. Remote Sens. Environ. 191, 419–432. https://doi.org/10.1016/j.rse.2016.12.022.

McGaughey, R.J., 2018. FUSION/LDV: Software for LiDAR Data Analysis and Visualization. Forest Service Pacific Northwest Research Station USDA, Seattle, WA, USA. Available online: http://forsys.cfr.washington.edu/fusion/FUSIONmanual.pdf (accessed on 15 October 2018).

Miller, J.D., Yool, S.R., 2002. Mapping forest post-fire canopy consumption in several overstory types using multi-temporal Landsat TM and ETM data. Remote Sens. Environ. 82, 481–496.

Miller, J.D., Thode, A.E., 2007. Quantifying burn severity in a heterogeneous landscape with a relative version of the delta normalized Burn Ratio (dNBR). Remote Sens. Environ. 109, 66–80.

Molina-Terrén, D.M., Cardil, A., Kobziar, L.N., 2016. Practitioner Perceptions of Wildland Fire Management across South Europe and Latin America. Forests 7, 184.

Montealegre, A.L., Lamelas, M.T., Tanase, M.A., de la Riva, J., 2014. Forest fire severity assessment using ALS data in a Mediterranean environment. Remote Sens. 6 (5), 4240–4265. https://doi.org/10.3390/rs6054240.

Næsset, E., 2002. Predicting forest stand characteristics with airborne scanning laser using a practical two-stage procedure and field data. Remote Sens. Environ. 80, 88–99.

NIFC, 2019. Federal Firefighting Costs (Suppression Only). Accessed August. 7 2019. https://www.nifc.gov/fireInfo/fireInfo_documents/SuppCosts.pdf.

Oliveras, I., Gracia, M., Moré, G., Retana, J., 2009. Factors influencing the pattern of fire severities in a large wildfire under extreme meteorological conditions in the Mediterranean basin. Int. J. Wildland Fire 18, 755–764. https://doi.org/10.1071/WF08070.

Pasher, J., King, D.J., 2009. Mapping dead wood distribution in a temperate hardwood forest using high resolution airborne imagery. For. Ecol. Manage. 258, 1536–1548.

Qi, J., Chehbouni, A., Huete, A.R., Kerr, Y.H., 1994. Modified soil adjusted vegetation index (MSAVI). Remote Sens. Environ. 48, 119–126.

R Core Team, 2019. R: A Language and Environment for Statistical Computing. R Foundation for Statistical Computing, Vienna, Austria Available online: http://www.R-project.org (Accessed on 15 July 2017).

Rothermel, Richard C., Rinehart, George C., 1983. Field procedures for verification and adjustment of fire behavior predictions. Gen. Tech. Rep. INT-142. U.S. Department of Agriculture, Forest Service, Intermountain Forest and Range Experiment Station, Ogden, UT 25 p.

Scott, Joe H., Reinhardt, Elizabeth D., 2001. Assessing crown fire potential by linking models of surface and crown fire behavior. Research Paper RMRS-RP-29. Rocky Mountain Research Station, USDA Forest Service, Fort Collins, CO 59 p.

Silva, C.A., Crookston, N.L., Hudak, A.T., Vierling, L.A., 2015. rLiDAR: An R Package for Reading, Processing and Visualizing LiDAR (Light Detection and Ranging) Data, Version 0.1. Accessed Oct. 15 2017. http://cran.rproject.org/web/packages/rLiDAR/index.html.

Silva, C.A., Hudak, A.T., Vierling, L.A., Loudermilk, E.L., O'Brien, J.J., Hiers, J.K., Jack, S.B., Gonzalez-Benecke, C., Lee, H., Falkowski, M.J., 2016. Imputation of individual longleaf pine (*Pinus palustris* mill.) tree attributes from field and LiDAR data. Can. J. Remote Sens. 42, 554–573.

Silva, C.A., Klauberg, C., Hudak, A.T., Vierling, L.A., Jaafar, W.S.W.M., Mohan, M., Garcia, M., Ferraz, A., Cardil, A., Saatchi, S., 2017. Predicting stem total and assortment volumes in an industrial Pinus taeda L. forest plantation using airborne laser scanning data and random forest. Forests 8, 254.

Skowronski, N.S., Clark, K.L., Duveneck, M., Hom, J., 2011. Three-dimensional canopy fuel loading predicted using upward and downward sensing LiDAR systems. Remote Sens. Environ. 115, 703–714.

Steininger, M., 2000. Satellite estimation of tropical secondary forest above-ground biomass: data from Brazil and Bolivia. Int. J. Remote Sens. 21 (6), 1139–1157.

Swetnam, T.L., Lynch, A.M., Falk, D.A., Yool, S.R., Guertin, D.P., 2015. Discriminating disturbance from natural variation with LiDAR in semi-arid forests in the southwestern USA. Ecosphere 6 (6), 97.

Tanase, M.A., Santoro, M., Wegmüller, U., de la Riva, J., Pérez-Cabello, F., 2010. Properties of X-, C- and L-band repeat-pass interferometric SAR coherence in Mediterranean pine forests affected by fires. Remote Sens. Environ. 114, 2182–2194.

Tanase, M., de la Riva, J., Santoro, M., Pérez-Cabello, F., Kasischke, E., 2011. Sensitivity of SAR data to post-fire forest regrowth in Mediterranean and boreal forests. Remote Sens. Environ. 115, 2075–2085.

Tucker, C.J., 1979. Red and photographic infrared linear combinations for monitoring vegetation. Remote Sens. Environ. 8, 127–150.

Turner, M.G., Hargrove, W.W., Gardner, R.H., Romme, W.H., 1994. Effects of fire on landscape heterogeneity inYellowstone National Park, Wyoming. J. Veg. Sci. 5, 731–742. https://doi.org/10.2307/3235886.

Vauhkonen, J., 2010. Estimating crown base height for Scots pine by means of the 3D geometry of airborne laser scanning data. Int. J. Remote Sens. 31 (5), 1213–1226. https://doi.org/10.1080/01431160903380615.

Veraverbeke, S., Lhermitte, S., Verstraeten, W.W., Goossens, R., 2011. Evaluation of pre/post-fire differenced spectral indices for assessing burn severity in a Mediterranean environment with Landsat Thematic Mapper. Int. J. Remote Sens. 32 (12), 3521–3537.

Verbyla, D., Lord, R., 2008. Estimating post-fire organic soil depth in the Alaskan boreal forest using the Normalized Burn Ratio. Int. J. Remote Sens. 29, 3845–3853.

Viera, A., Garrett, J., 2005. Understanding Interobserver Agreement The Kappa StatisticFamily Medicine Journalinterobserver agreement the kappa statistic. Fam. Med. J. 37, 360–363.

Vogeler, J.C., Yang, Z., Warren, B., 2016. Cohen. Mapping post-fire habitat characteristics through the fusion of remote sensing tools. Remote Sens. Environ. 173, 294–303.

Wing, B.M., Ritchie, M.W., Boston, K., Cohen, W.B., Olsen, M.J., 2015. Individual snag detection using neighborhood attribute filtered airborne lidar data. Remote Sens. Environ. 163, 165–179.

Willis, K.S., 2015. Remote sensing change detection for ecological monitoring in United States protected areas. Biol. Conserv. 182, 233–242.

Wulder, M.A., White, J.C., Alvarez, F., Han, T., Rogan, J., Hawkes, B., 2009. Characterizing boreal forest wildfire with multi-temporal Landsat and LIDAR data. Remote Sens. Environ. 113, 1540–1555.